CHINESE OPTICS LETTERS

Vol. 23, No. 1 | January 2025

Pattern control of a *Q*-switched pulsed laser with a dual-cavity configuration digital laser

Zheng-Xian Tsai (蔡政憲), Kuo-Chih Chang (張國誌), and Shu-Chun Chu (朱淑君)*

Department of Physics, National Cheng Kung University, Tainan 701, China

*Corresponding author: scchu@mail.ncku.edu.tw

Received March 20, 2024 | Accepted August 1, 2024 | Posted Online January 22, 2025

In this paper, a digital laser with a dual-cavity configuration for the pattern control of a *Q*-switched pulsed laser is presented. The dynamic pattern control of the pulsed laser from the primary cavity is generated and controlled by simply manipulating the projected phase of the spatial light modulator (SLM) in the secondary cavity. The proposed digital laser design provides a solution for a flexible pulsed laser source while preventing damage to the SLM from high-peak light pulse flux density, benefiting structured laser applications that require high-peak laser power.

Keywords: pulsed laser; structured beam; digital laser; intracavity beam shaping.

DOI: 10.3788/COL202523.011404

1. Introduction

Intracavity beam shaping is crucial in obtaining complex structured laser sources. Since Ngcobo *et al.* proposed digital lasers[1], intracavity shaping technology has flourished. Digital lasers are a new architecture that places the spatial light modulator (SLM) inside the cavity as a resonant cavity element, allowing it to control the amplitude and phase of the cavity in real time to select the desired mode. However, a previous study has shown that high-power incident light can cause SLM damage, including thermal damage and dielectric breakdown[2]. Particularly, high power density and short pulse incident light can potentially damage an SLM. The damage threshold of the SLM directly limits the output power of the digital laser. Therefore, research on digital lasers mainly centers on lower-power continuous-wave (CW) lasers[3–6].

Improving the output power of digital lasers is extremely valuable for expanding the applications of digital lasers. Notably, the dual-cavity laser system may provide a feasible solution for digital lasers to achieve high-power laser output. The dual-cavity laser configuration was first proposed by Arbabzadah *et al.*[7], who used a secondary laser cavity to control the gain in a *Q*-switched primary laser cavity and enabled clean single-pulse *Q*-switched TEM_{00} mode operation of high repetition rate. They extended the dual-cavity architecture to the laser pattern formation. As a result, CW flat-top beams[8,9] and Laguerre–Gaussian (LG) mode output[10,11] were achieved. Chen *et al.* were the first to apply the dual-cavity laser configuration to digital lasers[12]. The SLM panel was divided into two regions to form the boundary of two laser cavities, and two orthogonally polarized CW Hermite–Gaussian (HG) beams from two laser cavities were superimposed. This method resulted in several beam patterns and polarizations. However, this dual-cavity configuration cannot be operated in *Q*-switching mode by adding an inserted *Q*-switch optical element because the high intracavity peak intensity of the pulsed laser will cause damage to the SLM panel. Despite recent industrial advances resulting in significant improvements in SLM damage thresholds, the use of SLM in a high-peak-power pulsed laser cavity still carries the risk of dielectric damage.

In this study, we propose a new dual-cavity configuration for a digital laser system to successfully generate pulsed laser outputs for selected beam patterns. In particular, this study aims to achieve a pattern-selected pulsed laser output with higher peak flux density in the primary cavity through SLM phase modulation of a lower flux density CW laser in the secondary cavity. The proposed approach contributes to extending the output peak flux density of the structured pulsed laser generated in digital laser. This research expands the possibilities of digital lasers for applications of high-peak-power structured lasers.

2. Experimental Setup and Method

The proposed digital laser with a dual-cavity configuration and the laser light measurement setup are illustrated in Fig. 1. The laser system adopted an end-pumped laser configuration. The excitation light source was focused on a 3 mm × 3 mm × 5 mm, 1%-doped, Nd:YAG crystal, and the side facing the excitation light source had a coating (reflectance > 99.9% at 1064 nm). The secondary cavity was formed by the SLM panel, a polarization beam splitter (PBS), and the coated side of the

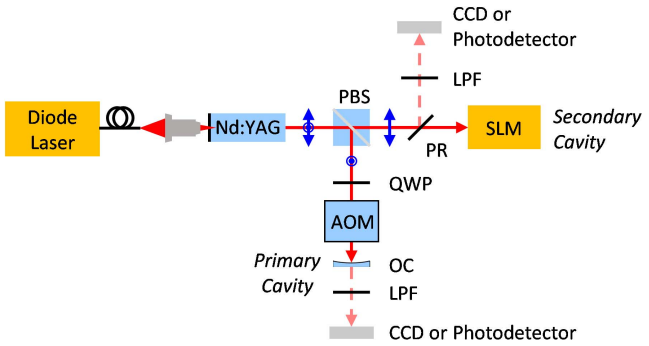

Fig. 1. Schematic diagram of the experimental setup for the dual-cavity configuration for mode-selective pulsed laser generation with a digital laser.

Nd:YAG laser crystal. Then, a partial reflector (PR) was inserted into the secondary cavity to observe the laser field pattern in the secondary cavity. The primary cavity was formed by the coated side of the laser crystal, a PBS, a quarter-wave plate (QWP), an acousto-optic modulator (AOM), and an output coupler (OC). The laser light paths of the primary cavity and the secondary cavity were separated by the PBS, where the S-polarized beam entered the primary cavity, and the P-polarized beam entered the secondary cavity. This mechanism ensured that the light field polarization of the secondary cavity aligned with the requirement of the SLM. In the secondary cavity, the selection of a CW lasing mode could be easily controlled by the known projected phase boundaries of the SLM[4,13,14]. In the primary cavity, the *Q*-switch operation was performed through the embedded AOM, allowing an actively *Q*-switched Nd: YAG laser to be formed in order to achieve a pulsed laser output. The role of the QWP was to adjust the laser threshold of the primary cavity. The modulation of the light field of the primary cavity passing through a QWP twice was equivalent to passing through a half-wave plate (HWP). By rotating the QWP to control the angle between its fast axis and the S-polarization direction, an adjustable loss was introduced.

The parameters of the laser system are listed in detail in this paragraph. For the secondary cavity, the SLM is a reflect-type phase-controlled liquid crystal modulator (LCOS-SLM X15213-03 R) manufactured by Hamamatsu Photonics, with 1280×1024 pixel number, 12.5×12.5 μm pixel size, 216 phase steps in 2π range, 96% fill factor, and 97% light-adopting efficiency. The transmittance of the PR was 97%, and the PBS diameter was 15 mm. The distance between the SLM panel and the Nd:YAG crystal was 22.5 cm. Meanwhile, the OC of the primary cavity was a concave mirror with a curvature radius of 25 cm and a transmittance of 8% for 1064 nm light. The distance between the OC and the PBS was 19.5 cm, and that between PBS and the Nd:YAG crystal was 3 cm. The length of the AOM crystal was 5.9 cm, with an acoustic center frequency of 40 MHz. The acoustic wave was modulated by an external 30 kHz TTL signal, which allowed the AOM to function as an on/off switch.

In this study, a quasi-continuous wave (QCW) 808 nm pumping light source with a duty cycle of 3% and a frequency of 100 Hz was used to minimize thermal effects[15–17] and prevent potential damage to the laser crystal from focused pumping. The input peak power ($P_{\mathrm{peak,in}}$) of QCW is bounded between 0 and 80 W, multiplied by 3% duty cycle to get its average input power ($P_{\mathrm{ave,in}}$). Two long pass filters (LPFs) were located in front of the observing equipment to remove the 808 nm pumping light. CCDs were used to measure the light-field pattern, which could be replaced by power meters or photodetectors (ALPHALAS, UPD-50-UP) to measure power and pulse signals, respectively.

The pattern selection of the pulsed laser in the primary cavity was achieved by controlling its laser gain spatial distribution through modulating the secondary cavity. Notably, the laser light paths of the two cavities completely overlapped in the laser crystal. In the dual-cavity laser system, the primary and the secondary cavities were related through the competition of a shared laser gain region[11]. In the experiments, the laser mode selection of the secondary cavity was controlled by changing the projection phase of the SLM. Concurrently, the loss of the primary laser cavity was fine-tuned through the rotating QWP, causing the secondary cavity to have a lower laser threshold than the primary cavity. Hence, the lasing state of the secondary cavity was achieved prior to the primary cavity–that is, the manipulation of the lasing mode in the secondary cavity was equivalent to controlling the remaining spatial distribution of laser gain that the primary cavity could use. This mechanism led to the success of spatial mode selection in the primary cavity. It is observed that the SLM provides considerable flexibility in controlling the laser mode of the secondary cavity–that is, the spatial distribution of laser gain within the primary cavity to arise in flexibility in the pulsed laser pattern selection.

3. Results and Discussion

Figure 2 shows the results of HG_{01} pulsed laser generation using the laser system. Figure 2(a) shows the central part of the SLM phase diagram that the secondary cavity adopted. Figures 2(b) and 2(c), respectively, present the laser field patterns obtained from the secondary cavity and the primary cavity. The beam size of the laser field in the primary cavity is larger than that in the secondary cavity. This is presumably due to the increased optical path length introduced by the AOM in the primary cavity. In the experiment, the threshold of the primary cavity is higher than that of the secondary cavity, and the output power of the secondary cavity is higher than that of the primary cavity. Consequently, the light field in Fig. 2(b) is brighter than that in Fig. 2(c). In the secondary cavity, the HG_{10} mode was controlled-selected by projecting a proper SLM phase diagram, which forced the HG_{01} mode laser of complementary light-field intensity to be generated in the primary cavity. The SLM projection phase design is as follows. The selected lasing HG_{10} field at SLM is numerically calculated, denoted by $\mathrm{HG}_{10} = A\ \exp(i\phi_{10})$, where A and ϕ_{10}, respectively, denote the amplitude and phase of the HG_{01} field. The loaded SLM diagram mainly provides phase modulation $M_p = \exp(-i2\phi_{10})$ that makes a reflected light field become a conjugate field of the incident HG_{10} field. This mechanism turns the secondary cavity into a stable cavity for

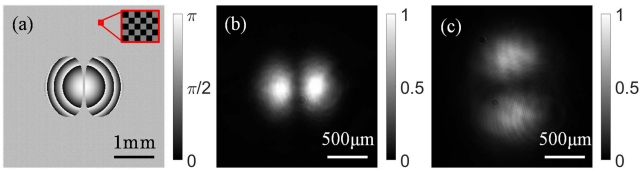

Fig. 2. Results for a pulsed HG_{01} mode generation. (a) Phase diagram projected on the SLM; the red box shows the 0-π checkerboard phase; (b) and (c) laser field intensities of the secondary and primary cavities, respectively.

the specified HG_{10} mode. In addition, in the range of the phase diagram corresponding to the region of the low-energy distribution of the HG_{10} field, a high diffraction loss is introduced with a 0-π checkerboard phase to prevent other cavity mode lasing.

Figure 3 shows more results in the pattern control of pulsed laser generation from the dual-cavity laser system. Figure 3(a) is the measured intensity distribution of the secondary cavity of controlled HG_{10}, HG_{01}, and HG_{00} modes, respectively. Figure 3(b) shows the pulsed laser patterns in the primary cavity corresponding to the secondary cavity with respective laser pattern in Fig. 3(a). The HG_{01} mode, the HG_{10} mode, and the ring-like pulsed laser are successfully generated with the dual-cavity digital laser. In the experiments, the laser light paths of the two cavities completely overlapped in the laser crystal–that is, two cavities share a laser gain of the same spatial distribution. When the HG_{10} mode is generated in the secondary cavity, it will exhaust the laser gain on the left and right sides before the primary cavity. Thus, the main cavity will only obtain laser gain in the upper and lower areas, forming the HG_{01} mode. The mechanism that produces an HG_{10} pulsed laser is the same as

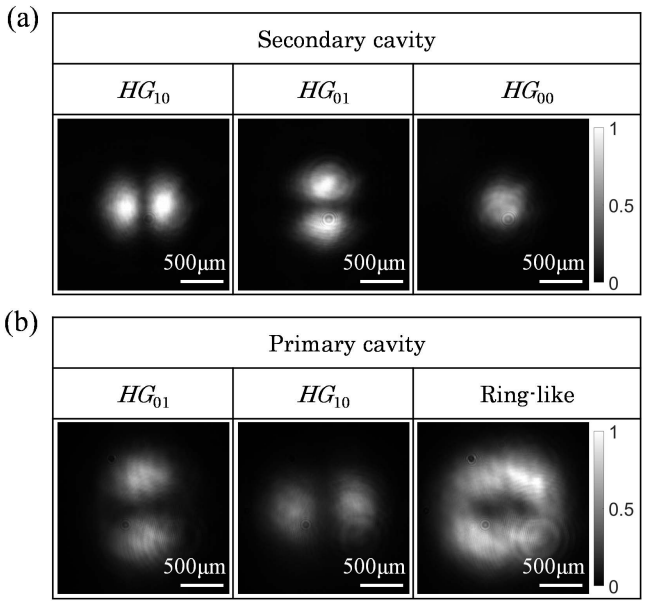

Fig. 3. Results for the pulsed laser generation with average input power of 2.4 W. (a) Measured laser intensity distribution from the secondary cavity–HG_{10}, HG_{01}, and HG_{00} CW laser; (b) pulsed laser patterns in the primary cavity accordingly.

that for generating an HG_{01} pulsed laser. When the HG_{00} mode is generated by the secondary cavity, it consumes the center region of the laser gain, enabling the primary cavity to produce a ring-like pattern effectively. In addition, supplementary data shows the dynamic control of the pulsed laser pattern of the primary cavity through the manipulation of the SLM projected phase diagram of the secondary cavity. By switching the orientation of the projected SLM phase diagram counterclockwise, the laser field patterns of the secondary cavity (left pattern) and the primary cavity (right pattern) changed accordingly. The results demonstrate that it is possible to use a secondary cavity to modulate the field pattern of the primary cavity. However, with a higher laser mode volume, the modal dependence between the primary and secondary cavities is expected to become more complex. To achieve more intricate and diverse laser patterns, adjusting the projection phase of the digital laser via laser output feedback may be necessary[18]. This is also a research direction worth exploring in the future.

The time characteristics of the pulsed laser in the primary cavity within the HG_{01} field pattern were measured and compared to the secondary cavity's characteristics in the generation of the HG_{10} CW laser. Figure 4 shows the laser output power of the two cavities versus the average input pump power. The laser output power of both cavities increases with increasing pump power. As expected, through the adjustment of the QWP placed in the primary cavity, the secondary cavity exhibited a lower laser threshold and prioritized laser emission more than the primary cavity. In this study, the laser threshold of the secondary cavity was close to 0.6 W, while the primary cavity was around 1.5 W. The laser field intensity patterns when the excitation power was 1.5 W are not shown in the figure because the laser output of the primary cavity was unstable near the laser threshold. It is important to note that the current efficiency is not optimal. The fundamental reason for this is that the pump source employs tight focusing, which results in the focus falling in the front

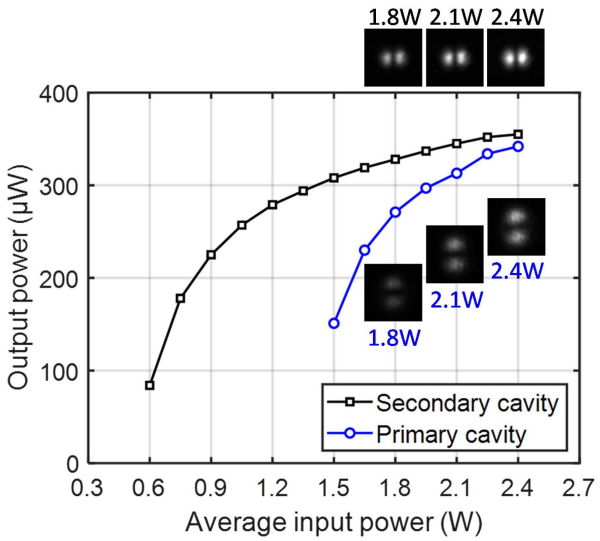

Fig. 4. Characteristics of laser output-input power of the two cavities (i.e., primary and secondary).

end of the crystal and diverging rapidly, thereby reducing the actual absorption of the pump power compared to the input power. This can be improved by modifying the pump design, which will not affect the concept or results of this study. The pulse characteristics of the primary cavity are presented in Fig. 5. Since the pulse is only generated when the pump source is in the "ON" state, the input peak power, rather than the average input power, is used as the horizontal axis of the coordinates. Figure 5(a) shows that the pulse full width at half-maximum (FWHM) decreases as the input peak power increases. Figure 5(b) provides the time profile of the laser pulse for the narrowest pulse width obtained ($P_{peak,in} = 80$ W) in this study. Figure 5(c) illustrates the relationship between pulse energy and $P_{peak,in}$ in the primary cavity. The single pulse energy in the primary cavity increases as the $P_{peak,in}$ increases. In the experiments, when the input peak power was 80 W, a laser pulse of the highest single-pulse energy of 342 nJ, a narrowest pulse width of 696 ns, and a maximum peak power of 0.49 W were obtained. Considering that the existing experimental architecture uses end-pumping and does not use mode-locking technology, the optical conversion efficiency, output power, and pulse power of the pulsed laser light obtained are not very high. These shortcomings can be further improved by changing the pumping method[19] and using mode-locking technology[20]. Figure 5(d) presents a plot of the primary cavity's peak laser power ratio to the CW laser power of the secondary cavity. With increasing input power, the increase in peak power obtained in the primary cavity was greater than the increase in laser power obtained in the secondary cavity.

Figure 6 shows the comparison of the intracavity light power per area (i.e., radiant flux density) between the primary and secondary cavities with the safe values of the SLM adopted in this study, where the intracavity light power per area was calculated

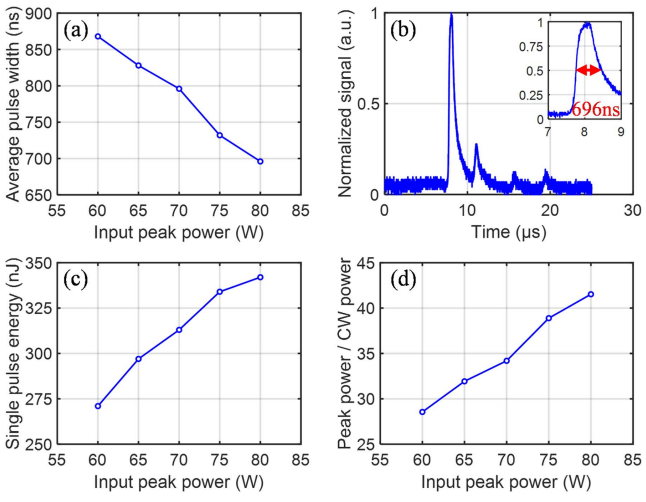

Fig. 5. Characteristics of the laser pulse from the primary cavity versus input peak power. (a) Average pulse width; (b) time profile at input peak power of 80 W; (c) single-pulse energy; (d) ratio of the primary cavity peak power to the secondary cavity CW power.

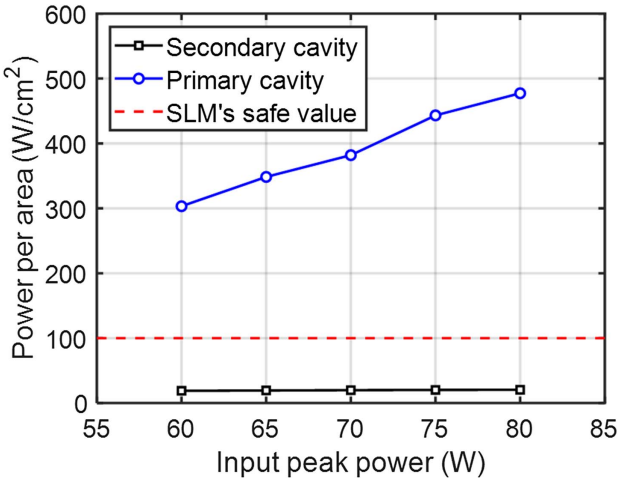

Fig. 6. Comparison of power per area for the primary and secondary cavities and safe values for SLM.

by dividing the intracavity light power with the laser beam waist area[2]. Figure 6 reveals that the dual-cavity configuration in this study allowed the SLM to be safely operated below its safe value by performing safe SLM phase modulation with a CW laser of lower flux density in the secondary cavity while achieving a pattern-selective pulsed laser output with higher peak flux density in the primary cavity. With the improvement of manufacturing technology, the power threshold of SLM continues to increase. SLM might be directly placed into the pulse laser cavity for future use. Since SLMs invariably have limited power thresholds, the dual-cavity method reported in this study helps to expand the output peak flux density of the structured laser generation of the digital laser. The proposed dual-cavity configuration provides a possible solution for successfully dynamic pattern selection of the pulsed laser while preventing damage to the SLM with a high-peak light pulse flux density.

4. Conclusion

This study proposes what we believe is the first digital laser with a dual-cavity configuration for pattern-selective pulsed laser generation. The dynamic pattern selection of the pulsed laser was achieved by the effective spatial/lateral laser gain control of the primary cavity, achieved through the secondary cavity laser mode selection with a pure phase modulation of an intracavity SLM. Although the power demonstrated in this study was not particularly high, the proposed dual-cavity configuration successfully achieved dynamic pattern selection of a pulsed laser while preventing the SLM from directly experiencing high-peak light pulse flux density. This allowed the SLM to avoid pulse-induced dielectric damage. The generation of the pulsed HG_{01} mode with arbitrary orientation and a donut-like pulsed laser was demonstrated with the proposed dual-cavity digital laser configuration. More laser patterns of pulsed laser outputs could be achieved through mature cavity mode selection methods for digital lasers[18], which could be further explored in the future.

Furthermore, the proposed digital laser configuration provides a controllable pulsed laser source for many applications requiring high-peak flux density (e.g., photolithography). Other pulsed laser technologies, such as mode locking or pulsed compression, can also further increase the generated pulsed laser peak flux density and are worth further exploration in the future.

Acknowledgements

This work was supported by the National Science and Technology Council, Taiwan, China (No. NSTC 112-2112-M-006-018).

References

1. S. Ngcobo, I. Litvin, L. Burger, *et al.*, "A digital laser for on-demand laser modes," Nat. Commun. **4**, 2289 (2013).
2. C. Sergio and B. Kipp, "Power handling for LCoS spatial light modulators," Proc. SPIE **10518**, 105181R (2018).
3. T. Bell, A. Hasnaoui, K. Ait-Ameur, *et al.*, "Excitation of high-radial-order Laguerre-Gaussian modes in a solid-state laser using a lower-loss digitally controlled amplitude mask," J. Opt. **19**, 105604 (2017).
4. C.-Y. Huang, K.-C. Chang, and S.-C. Chu, "Experimental investigation of generating laser beams of on-demand lateral field distribution from digital lasers," Materials **12**, 2226 (2019).
5. S.-C. Chu, Y.-X. Fu, K.-C. Chang, *et al.*, "Generating a geometric structure light field from a digital laser by specifying a laser cavity phase boundary with a Gaussian-convoluted target field," Opt. Express **29**, 35980 (2021).
6. L. L. Nguyen Thi and S.-C. Chu, "Generation of on-demand quasi-Mathieu beams with a controlled generation of spatial spectrum of angular Mathieu-Gauss functions with a digital laser," Opt. Express **30**, 5283 (2022).
7. E. A. Arbabzadah, P. C. Shardlow, A. Minassian, *et al.*, "Pulse control in a Q-switched Nd:YVO_4 bounce geometry laser using a secondary cavity," Opt. Lett. **39**, 3437 (2014).
8. D. J. Kim, J. I. Mackenzie, and J. W. Kim, "Adaptable beam profiles from a dual-cavity Nd:YAG laser," Opt. Lett. **41**, 1740 (2016).
9. E. Song, T. Dai, G. Zhu, *et al.*, "Adjustable and stable beam profile generation in a Yb:YAG thin-disk laser," Opt. Lett. **45**, 6550 (2020).
10. D. J. Kim and J. W. Kim, "Dual-cavity Nd:YAG laser with Laguerre-Gaussian (LG0n) mode output," Opt. Commun. **383**, 26 (2017).
11. W. R. Kerridge-Johns and M. J. Damzen, "Vortex laser from anti-resonant ring coupled cavities," Opt. Express **26**, 32839 (2018).
12. X. Chen, S. Liu, Z. Lin, *et al.*, "Dual-cavity digital laser for intra-cavity mode shaping and polarization control," Opt. Express **26**, 18182 (2018).
13. K.-F. Tsai and S.-C. Chu, "Numerical study on the selective excitation of Helmholtz–Gauss beams in end-pumped solid-state digital lasers with the control of the laser gain transverse position provided by off-axis end pumping," Laser Phys. **28**, 035801 (2018).
14. K.-F. Tsai and S.-C. Chu, "Generating laser output with arbitrary lateral shape by using multi-point beam superposition method in digital lasers," Laser Phys. **28**, 075801 (2018).
15. H. Sakai, A. Sone, H. Kan, *et al.*, "Polarization stabilizing for diode-pumped passively Q-switched Nd:YAG microchip lasers," in *Advanced Solid-State Photonics, Technical Digest* (2006), paper MD2.
16. R. Bhandari and T. Taira, "6 MW peak power at 532 nm from passively Q-switched Nd:YAG/Cr^{4+}:YAG microchip laser," Opt. Express **19**, 19135 (2011).
17. L. Zheng, A. Kausas, and T. Taira, "Drastic thermal effects reduction through distributed face cooling in a high power giant-pulse tiny laser," Opt. Mater. Express **7**, 3214 (2017).
18. C. Hu, Y. Xiao, Y. He, *et al.*, "Optimization of brightness in a Nd:YAG laser by maximizing the single-mode power factor with an intra-cavity spatial light modulator," Appl. Opt. **61**, 1482 (2022).
19. M. Messner, A. Heinrich, C. Hagen, *et al.*, "Acousto-optically Q-switched diode side-pumped Er:YLF laser generating 50-kW peak power in 70-ns pulses," Proc. SPIE **10896**, 1089607 (2019).
20. V. E. Nadtocheev and O. E. Naniĭ, "Use of traveling acoustic waves for mode locking in lasers," Sov. J. Quantum Electron. **19**, 1435 (1989).